Semiconducting ferroelectric photovoltaics through Zn^{2+} doping into $KNbO_3$ and polarization rotation

Fenggong Wang,* Ilya Grinberg, and Andrew M. Rappe†

The Makineni Theoretical Laboratories, Department of Chemistry, University of Pennsylvania, Philadelphia, Pennsylvania 19104-6323, USA

(Received 11 March 2014; revised manuscript received 13 May 2014; published 5 June 2014)

We demonstrate a new band engineering strategy for the design of semiconductor perovskite ferroelectrics for photovoltaic and other applications from first principles. We study six ferroelectric solid solutions created by partially substituting Zn^{2+} for Nb^{5+} into the parent $KNbO_3$ material, combined with charge compensation at the A sites with different combinations of higher valence cations. Our first-principles calculations with the HSE06 functional yield a low band gap of only 2.1 eV for the 75%$KNbO_3$-25%$(Sr_{1/2}La_{1/2})(Zn_{1/2}Nb_{1/2})O_3$ solid solution, and this can be lowered further by 0.6 eV under strain through polarization rotation. The large polarization, especially under strain, of these materials provides a charge separation route by the bulk photovoltaic effect that could potentially allow power conversion efficiency beyond the Shockley-Queisser limit. This band engineering strategy is applicable to other perovskites and should be realizable by standard solid-state synthesis and thin film growth methods.

DOI: 10.1103/PhysRevB.89.235105 PACS number(s): 72.80.Ga, 77.55.fj, 77.84.Bw

I. INTRODUCTION

Solar energy is the most promising long-term source of clean, renewable energy to replace the traditional energy reliance on fossil fuels [1]. Unfortunately, the solar cell power conversion efficiency (PCE) is limited by the Shockley-Queisser limit in conventional solar cells, in which the excited carriers are separated by the internal electric field at a p-n junction or other material interface [2]. Ferroelectrics possess an intrinsic spontaneous polarization, and this provides an alternative way to separate charge by the bulk of the material [3,4]. This is called the bulk photovoltaic effect, since charge carriers are separated by a single phase material [5,6]. Time-dependent perturbation theory analysis clearly manifests the roles of broken inversion symmetry and spontaneous charge separation in bulk photovoltaic effect [7]. Furthermore, ferroelectric oxides are stable in a wide range of mechanical, chemical, and thermal conditions and can be synthesized using low-cost methods such as sol-gel and sputtering. Therefore, ferroelectric ABO_3 perovskite oxides such as $BiFeO_3$ and $Pb(Zr_{1/2}Ti_{1/2})O_3$ (PZT) have been broadly explored to increase the PCE [4,8–18]. Further improvement of the PCE has been impeded by the wide band gaps (E_g >2.7 eV for $BiFeO_3$, E_g >3.5 eV for PZT) of ferroelectric oxides, which allow the use of only 8%–20% of the solar spectrum. This has inspired theoretical design/engineering and experimental demonstration of low-band-gap ferroelectric oxides, e.g., by chemical substitution in a solid solution [19–30]. In particular, a weakly ferroelectric nonperovskite $KBiFe_2O_5$ with a band gap of 1.6 eV [13] and a ferroelectric oxide $(K,Ba)(Ni,Nb)O_{3-\delta}$ with a direct band gap of 1.39 eV have been reported very recently [31]. In $(K,Ba)(Ni,Nb)O_{3-\delta}$, the combination of low gap and polarization is achieved through ferroelectrically active Nb ions providing the polarization combined with Ni^{2+} and oxygen vacancies lowering the band gap into the visible range.

However, this new ferroelectric oxide relies on the presence of a large concentration of oxygen vacancies. This is detrimental to polarization switching and can also trap the photogenerated carriers and increase the charge recombination rate. This motivates us to investigate alternative band structure engineering approaches to lower E_g while preserving ferroelectricity. Previous theoretical studies have shown that the valence band maxima (VBM) of Zn-containing oxides can be shifted up through the repulsion between the nonbonding Zn $3d$ orbitals and O charge densities in the presence of extreme tetragonality or oxygen vacancies [32]. While this decreases E_g, extreme tetragonality or high O-vacancy content can be difficult to achieve experimentally. In this study, we show how a local valence imbalance created by Zn substitution for a higher-valence B cation in $KNbO_3$ gives rise to increased O $2p$-Zn $3d$ repulsion and higher VBM. The sensitivity of the conduction band minimum (CBM) to the direction of the local B-site atom off centering is used to further decrease E_g. Combined, the two effects lower the E_g of the parent $KNbO_3$ material by 2.04 eV in HSE06 calculations, moving it into the visible range.

The parent $KNbO_3$ material is used to provide the B-site cation off-center displacements and polarization. To maintain overall charge neutrality, we couple Zn substitution on the B site with A_1^{2+} and A_2^{3+} substitution on the A site ($A_1^{2+} = Pb^{2+}$, Ba^{2+}, Sr^{2+}, $A_2^{3+} = La^{3+}$, Bi^{3+}). We study a total of six $KNbO_3$-based solid solutions in fully relaxed and in strained configurations, including $(1-x)KNbO_3$-$x(Sr_{1/2}Bi_{1/2})(Zn_{1/2}Nb_{1/2})O_3$ (KN-SBZN), $(1-x)KNbO_3$-$x(Ba_{1/2}Bi_{1/2})(Zn_{1/2}Nb_{1/2})O_3$ (KN-BBZN), $(1-x)KNbO_3$-$x(Pb_{1/2}Bi_{1/2})(Zn_{1/2}Nb_{1/2})O_3$ (KN-PBZN), $(1-x)KNbO_3$-$x(Sr_{1/2}La_{1/2})(Zn_{1/2}Nb_{1/2})O_3$ (KN-SLZN), $(1-x)KNbO_3$-$x(Ba_{1/2}La_{1/2})(Zn_{1/2}Nb_{1/2})O_3$ (KN-BLZN), and $(1-x)KNbO_3$-$x(Pb_{1/2}La_{1/2})(Zn_{1/2}Nb_{1/2})O_3$ (KN-PLZN). The Pb and Bi atoms make covalent bonds to the O atoms and are highly ferroelectrically active, whereas the Sr, Ba, and La atoms make ionic bonds to the O atoms

*fenggong@sas.upenn.edu
†rappe@sas.upenn.edu

and typically do not exhibit large off-center displacements. This allows us to explore how the A-site atomic off-center displacements and bonding character affect the O $2p$-Zn $3d$ repulsion and the overall electronic structure.

II. METHODS

To examine the microscopic structural and electronic properties of these solid solutions, we performed first-principles density functional theory (DFT) calculations using 40-atom ($2 \times 2 \times 2$) supercells. One of the eight B-site Nb^{5+} ions is replaced with Zn^{2+}, and two of the eight K^+ ions with the largest distance from each other are replaced with the A_1^{2+} and A_2^{3+} ions, respectively. This corresponds to the solid solution of $x = 0.25$.

We performed plane-wave DFT calculations within the local density approximation (LDA), as implemented in the QUANTUM-ESPRESSO code [33–35]. All elements are represented by norm-conserving, optimized nonlocal pseudopotentials with a cutoff energy of 50 Ry, generated with the OPIUM package [36]. Full structural optimizations were performed using $6 \times 6 \times 6$ Monkhorst-Pack k-point grids [37]. $8 \times 8 \times 8$ k-point grids were used for the density of states (DOS) calculations, while the polarization was calculated by the Berry phase approach with $6 \times 6 \times 20$ k-point grids, where the denser direction was permuted in order to calculate all three polarization components [38,39]. In order to avoid the unphysical delocalization of the strongly correlated d orbitals, we also used the DFT + U and HSE06 methods to improve the band-gap description [40–42]. In DFT + U, the Hubbard U is parameterized by the linear-response approach [43], while in HSE06 the exact exchange proportion is $\alpha = 0.25$. For Nb $4d$, we find $U = 3.55$ eV. For fully occupied Pb $5d$ and Zn $3d$ orbitals, the linear response approach yields $U = 0$. Our LDA calculations underestimate the structural tetragonality c/a by only 0.3%, and we therefore use the LDA optimized structures for all the electronic structure calculations.

III. RESULTS AND DISCUSSIONS

Several trends are clear from the inspection of the HSE06 band gaps of the KN-A_1A_2ZN solid solutions plotted as a function of the calculated Berry phase polarization (Fig. 1). First, all of the solid solutions possess smaller band gaps than the parent rhombohedral phase $KNbO_3$, with E_g decreasing by 0.62–1.43 eV. Second, we see a clear trend that the larger P values correlate with larger band gaps. Third, the larger P values are associated with the ferroelectrically active Pb and Bi cations on the A site. We also study the effect of cation arrangement and find that it has no significant effect on either the band gap or the polarization.

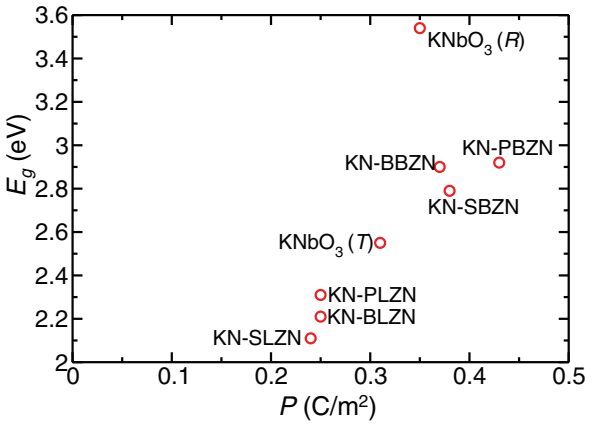

FIG. 1. (Color online) The HSE06 band gaps as a function of polarization for the designed solid solutions in fully relaxed configurations, including $(1-x)KNbO_3$-$x(Sr_{1/2}Bi_{1/2})(Zn_{1/2}Nb_{1/2})O_3$ (KN-SBZN), $(1-x)KNbO_3$-$x(Ba_{1/2}Bi_{1/2})(Zn_{1/2}Nb_{1/2})O_3$ (KN-BBZN), $(1-x)KNbO_3$-$x(Pb_{1/2}Bi_{1/2})(Zn_{1/2}Nb_{1/2})O_3$ (KN-PBZN), $(1-x)KNbO_3$-$x(Sr_{1/2}La_{1/2})(Zn_{1/2}Nb_{1/2})O_3$ (KN-SLZN), $(1-x)KNbO_3$-$x(Ba_{1/2}La_{1/2})(Zn_{1/2}Nb_{1/2})O_3$ (KN-BLZN), and $(1-x)KNbO_3$-$x(Pb_{1/2}La_{1/2})(Zn_{1/2}Nb_{1/2})O_3$ (KN-PLZN). Both rhombohedral (R) and tetragonal (T) $KNbO_3$ are shown for comparison.

Compared to LDA, the LDA + U method increases the band gaps of the Zn-based solid solutions by 0.25–0.39 eV while the HSE06 method increases them by 1.15–1.30 eV (Table I). Comparison with experimental $KNbO_3$ and ZnO band gaps shows that HSE06 is highly accurate for $KNbO_3$ but underestimates the ZnO band gap by 0.55–0.75 eV [44]. This suggests that HSE06 could also underestimate the band gaps of KN-A_1A_2ZN solid solutions. Nevertheless, the consistency in E_g differences for different functionals suggests that our calculations accurately capture the trend of the band gap change with different A-site substitutions. KN-SLZN is the most promising solid solution, exhibiting a low gap [45] while maintaining substantial polarization.

TABLE I. The band gaps E_g (eV) calculated with different methods and the polarization P (C/m^2) of various $KNbO_3$-based solid solutions, including $(1-x)KNbO_3$-$x(Sr_{1/2}Bi_{1/2})(Zn_{1/2}Nb_{1/2})O_3$ (KN-SBZN), $(1-x)KNbO_3$-$x(Ba_{1/2}Bi_{1/2})(Zn_{1/2}Nb_{1/2})O_3$ (KN-BBZN), $(1-x)KNbO_3$-$x(Pb_{1/2}Bi_{1/2})(Zn_{1/2}Nb_{1/2})O_3$ (KN-PBZN), $(1-x)KNbO_3$-$x(Sr_{1/2}La_{1/2})(Zn_{1/2}Nb_{1/2})O_3$ (KN-SLZN), $(1-x)KNbO_3$-$x(Ba_{1/2}La_{1/2})(Zn_{1/2}Nb_{1/2})O_3$ (KN-BLZN), and $(1-x)KNbO_3$-$x(Pb_{1/2}La_{1/2})(Zn_{1/2}Nb_{1/2})O_3$ (KN-PLZN). The corresponding values of the parent $KNbO_3$ in tetragonal (T), orthorhombic (O), and rhombohedral (R) phases are also shown. The number in parentheses is the experimental polarization.

	KN-BLZN	KN-SLZN	KN-PLZN	KN-BBZN	KN-SBZN	KN-PBZN	$KNbO_3$ (T)	$KNbO_3$ (O)	$KNbO_3$ (R)
E_g^{LDA}	1.05	0.93	1.10	1.60	1.56	1.75	1.40	1.63	2.24
E_g^{LDA+U}	1.43	1.32	1.48	1.85	1.91	2.00	1.82	2.26	2.61
E_g^{HSE06}	2.21	2.11	2.31	2.90	2.79	2.92	2.55	3.15	3.54
P^{LDA}	0.25	0.24	0.25	0.37	0.38	0.43	0.31		0.35(0.41)

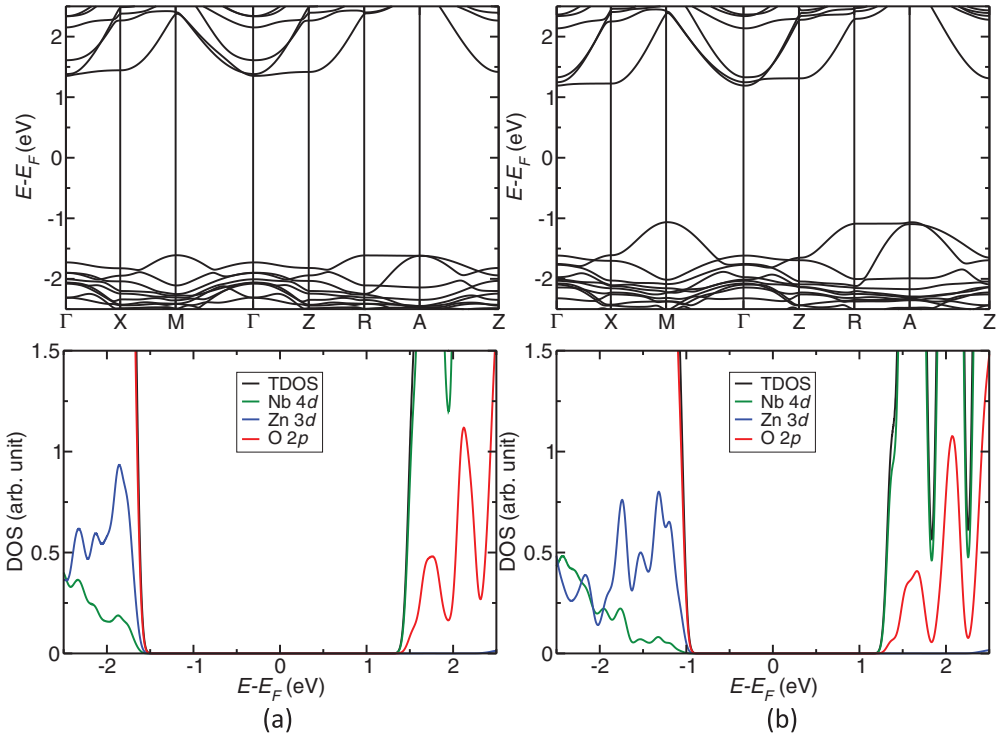

FIG. 2. (Color online) The band structure and total and projected density of states (TDOS and PDOS, respectively) of (a) $(1-x)KNbO_3$-$x(Pb_{1/2}Bi_{1/2})(Zn_{1/2}Nb_{1/2})O_3$ (KN-PBZN) and (b) $(1-x)KNbO_3$-$x(Sr_{1/2}La_{1/2})(Zn_{1/2}Nb_{1/2})O_3$ (KN-SLZN) solid solutions, respectively.

We now use KN-PBZN and KN-SLZN as examples to examine the origin of E_g decrease in the KN-A_1A_2ZN solutions (Fig. 2). Both KN-PBZN and KN-SLZN possess indirect band gaps, and their HSE06 band gaps are 2.92 and 2.11 eV, respectively. For both, the CBM consists mainly of the Nb 4d states, and their CB dispersions are largely identical. This confirms our expectation that the CBM is essentially preserved from the parent $KNbO_3$ to the newly designed solid solutions. However, their VBs show different bandwidths, with the VBs of KN-SLZN having greater dispersion, leading to a lower band gap. In both KN-PBZN and KN-SLZN, the VBM is composed of O 2p and Zn 3d states. Therefore, the Zn substitution for the higher-valence Nb leads to the presence of Zn 3d states at the VBM and a decrease in E_g.

Comparison of structural and electronic properties of KN-PBZN and KN-SLZN elucidates the role of O 2p-Zn 3d repulsion on band-gap reduction and shows how the ionic (or covalent) character and off-center displacements of the A-site cations affect the band gap. Projected density of states (PDOS) analysis shows that the O 2p orbitals are at three different positions of the VB depending on the atomic positions of O with respect to Zn, while all the Nb 4d orbitals are at almost the same energy position (Fig. 3). The O atoms that contribute orbitals to the VBM are adjacent to Zn, corresponding to the strongest Zn 3d-O 2p repulsion, whereas it is less significant for the O atoms that do not directly bond to Zn. This reflects the strength of O 2p-Zn 3d repulsion in determining the VBM positions [46]. These O atoms adjacent to Zn^{2+} ions are severely underbonded. The underbonding in KN-PBZN is less severe than in KN-SLZN because Pb and Bi cations tend to make large off-center displacements and create short, strong Pb-O and Bi-O bonds that mostly compensate the loss of B-O

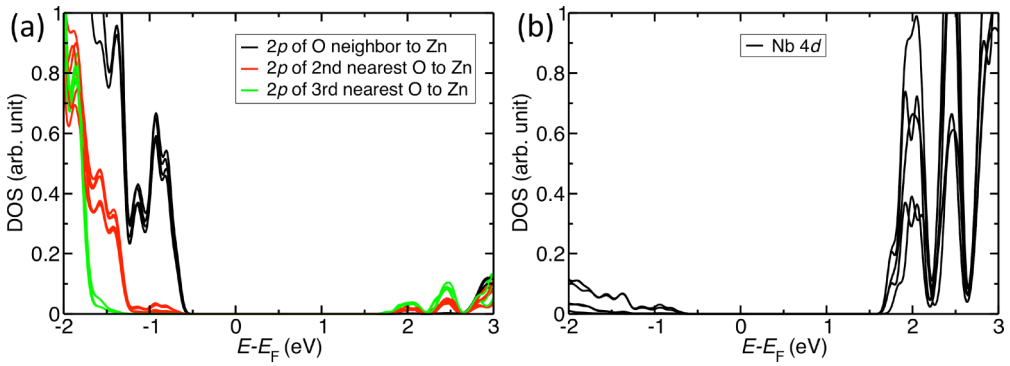

FIG. 3. (Color online) The PDOS onto (a) 2p orbitals of every O atom; and (b) 4d orbitals of every Nb atom in $(1-x)KNbO_3$-$x(Sr_{1/2}La_{1/2})(Zn_{1/2}Nb_{1/2})O_3$ (KN-SLZN).

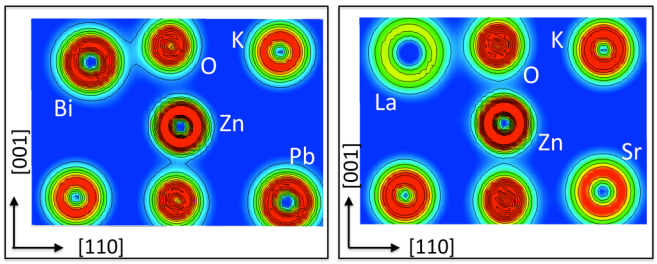

FIG. 4. (Color online) The charge density contours ($e/Å^2$) of $(1-x)KNbO_3$-$x(Pb_{1/2}Bi_{1/2})(Zn_{1/2}Nb_{1/2})O_3$ (KN-PBZN) and $(1-x)KNbO_3$-$x(Sr_{1/2}La_{1/2})(Zn_{1/2}Nb_{1/2})O_3$ (KN-SLZN). The Bi-O bonding is stronger than the La-O bonding, leading to a greater buildup of charge on the O atom adjacent to Zn in KN-SLZN than in KN-PBZN. This, in turn, leads to a larger overlap with the nonbonding Zn 3*d* states and an upshift in their energies, raising the energy of the VBM.

bonding due to replacement of Nb with Zn [32]. Furthermore, Löwdin analysis shows that the O atoms adjacent to Zn are more negative in KN-SLZN than in KN-PBZN (−0.75 vs −0.71) because of the ionic nature of Sr and La. Thus, the rise of the VBM is increased when *A*-cation displacements are reduced, giving more severe O underbonding and more ionicity (negative charge). These observations can be explained by the following bonding rearrangement mechanism.

The replacement of Nb^{5+} by Zn^{2+} creates a deficit of *B*-O bonding for the six O atoms that form the ZnO_6 cage. The lower valence on the *B* site is compensated by the replacement of two K^+ ions with A_1^{2+} and A_2^{3+} cations, making the *A*-O bonds stronger. However, at low A_1A_2ZN fractions, there are not enough substituted A_1^{2+} and A_2^{3+} cations to enhance *A*-O bonds for all six O atoms adjacent to Zn. Thus, this enhancement of *A*-O bonding cannot fully compensate the lost *B*-O bonding, leaving some O atoms with a buildup of nonbonding charge density. The overlap between the nonbonding O charge densities and the Zn 3*d* states raises the energies of the O and Zn states, moving the VBM up and lowering E_g with respect to the parent $KNbO_3$. The underbonding is less severe in KN-PBZN, where the Bi-O and Pb-O bonds draw O charge onto the Bi and Pb atoms and away from Zn, due to the ability of the Pb and Bi cations to make large off-center displacements and covalent bonds (Fig. 4). By contrast, the Sr and La atoms do not off center strongly and are less able to compensate the decrease of *B*-O bonding. As a result, the repulsion between the nonbonding O charge densities and Zn 3*d* states is stronger, leading to a larger VBM upshift in KN-SLZN. Additionally, the more ionic nature of Sr and La cations makes the O atoms more ionic, and this is also beneficial for the VBM upshift. This mechanism suggests that the larger displacement and covalency of Bi compared to those of La will lead to higher band gaps for KN-A_1BZN than for KN-A_1LZN, as is confirmed by our DFT calculations.

While the Zn^{2+} doping lowers the band gaps significantly, they are still fairly high (the lowest one is 2.11 eV for KN-SLZN by HSE06), especially when taking into account the underestimation of E_g for ZnO and other Zn-containing systems even by HSE06 [44]. We therefore use an additional band engineering strategy to further lower the band gaps into the visible light range. The local *P* direction in covalent ABO_3 perovskites is closely related with the band gap [47]. This can be seen for $KNbO_3$ as well, with a band-gap difference as large as 0.99 eV between the [111] (rhombohedral) and [001] (tetragonal) polarized $KNbO_3$ (Table I). The new KN-A_1A_2ZN solid solutions all exhibit locally [111] polar structures that are similar to the parent $KNbO_3$ material. We therefore apply in-plane compressive strains to rotate the local polarization toward the [001] direction in order to decrease the band gap. We find that compressive strain rotates the local polarization vector from [111] to [001] (Fig. 5). Concurrently, the HSE06 band gaps are reduced by 0.44–0.52 eV under 1% compressive strain and by a further 0.10–0.20 eV under 2% strain (Table II and Supplemental Material [48]). This will undoubtedly reduce the band gaps well into the visible light range even after the correction for possible band-gap underestimation is made.

Analysis of the band structure of strained KN-A_1A_2ZN solid solutions shows that further E_g reduction by strain is due to two factors: (1) The VBM is higher because the *p*-*d* repulsion is enhanced as the O-Zn-O angles have smaller deviations from 180°; (2) the CBM is lower because

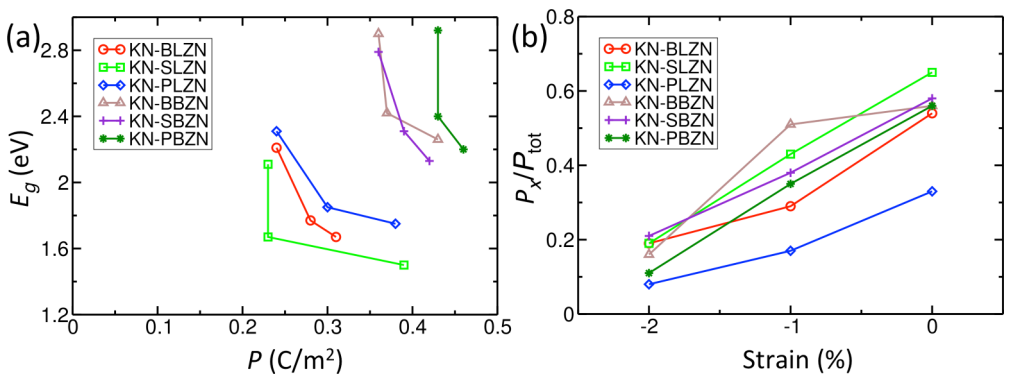

FIG. 5. (Color online) The (a) HSE06 band gap E_g as a function of the polarization *P* and (b) ratio between the *x* component of *P* and the total *P* (P_x/P_{tot}) of different $KNbO_3$-based solid solutions, including $(1-x)KNbO_3$-$x(Sr_{1/2}Bi_{1/2})(Zn_{1/2}Nb_{1/2})O_3$ (KN-SBZN), $(1-x)KNbO_3$-$x(Ba_{1/2}Bi_{1/2})(Zn_{1/2}Nb_{1/2})O_3$ (KN-BBZN), $(1-x)KNbO_3$-$x(Pb_{1/2}Bi_{1/2})(Zn_{1/2}Nb_{1/2})O_3$ (KN-PBZN), $(1-x)KNbO_3$-$x(Sr_{1/2}La_{1/2})(Zn_{1/2}Nb_{1/2})O_3$ (KN-SLZN), $(1-x)KNbO_3$-$x(Ba_{1/2}La_{1/2})(Zn_{1/2}Nb_{1/2})O_3$ (KN-BLZN), and $(1-x)KNbO_3$-$x(Pb_{1/2}La_{1/2})(Zn_{1/2}Nb_{1/2})O_3$ (KN-PLZN). In-plane compressive strain reduces E_g, increases *P*, and reduces the *x* component of *P*.

TABLE II. The HSE06 band gaps (eV) of various solid solutions under different in-plane compressive strains, including $(1-x)KNbO_3$-$x(Sr_{1/2}Bi_{1/2})(Zn_{1/2}Nb_{1/2})O_3$ (KN-SBZN), $(1-x)KNbO_3$-$x(Ba_{1/2}Bi_{1/2})(Zn_{1/2}Nb_{1/2})O_3$ (KN-BBZN), $(1-x)KNbO_3$-$x(Pb_{1/2}Bi_{1/2})(Zn_{1/2}Nb_{1/2})O_3$ (KN-PBZN), $(1-x)KNbO_3$-$x(Sr_{1/2}La_{1/2})(Zn_{1/2}Nb_{1/2})O_3$ (KN-SLZN), $(1-x)KNbO_3$-$x(Ba_{1/2}La_{1/2})(Zn_{1/2}Nb_{1/2})O_3$ (KN-BLZN), and $(1-x)KNbO_3$-$x(Pb_{1/2}La_{1/2})(Zn_{1/2}Nb_{1/2})O_3$ (KN-PLZN).

Strain	KN-BLZN	KN-SLZN	KN-PLZN	KN-BBZN	KN-SBZN	KN-PBZN
0	2.21	2.11	2.31	2.90	2.79	2.92
−1%	1.77	1.67	1.85	2.42	2.31	2.40
−2%	1.67	1.50	1.75	2.26	2.13	2.20

it has more nonbonding and less antibonding character in [001] polarized solid solutions [47,49]. The polarizations are enhanced concurrently with the band-gap reductions for all the solid solutions studied.

IV. CONCLUSIONS

In summary, we use first-principles calculations to demonstrate a new strategy for band engineering in perovskite ferroelectrics and show that it can be used to achieve ferroelectric materials with band gaps in the visible range. Six $KNbO_3$-based solid solutions are designed by doping Zn^{2+} ions into the parent $KNbO_3$ material, together with charge compensation by different combinations of higher-valence *A*-site cations. In particular, HSE06 hybrid functional calculations show a low band gap of only 2.11 eV for KN-SLZN, and this can be lowered further by 0.54–0.72 eV with strain. So, the lowest band gap (2.05–2.25 eV with strain) of the newly designed solid solutions (KN-SLZN) can be well within the visible light range even after considering that HSE06 may still underestimate the band gaps of Zn-containing materials by 0.55–0.75 eV. In addition, the preservation or enhancement under strain of the polarization makes these solid solutions, especially the La^{3+}-doped ones, very promising for bulk photovoltaic energy conversion. The strategy demonstrated here does not rely on exotic structure or the presence of oxygen vacancies and can be applied to other perovskite ferroelectrics.

ACKNOWLEDGMENTS

F.W. was supported by the National Science Foundation, under Grant No. DMR11-24696. I. G. was supported by the Office of Naval Research, under Grant No. N00014-12-1-1033. A.M.R. was supported by the Department of Energy under Grant No. DE-FG02-07ER46431. Computational support was provided by the High-Performance Computing Modernization Office of the Department of Defense and the National Energy Research Scientific Computing Center of the Department of Energy. We thank Professor Peter K. Davies for fruitful discussions.

[1] K. Maeda, K. Teramura, D. Lu, T. Takata, N. Saito, Y. Inoue, and K. Domen, Nature (London) **440**, 295 (2006).
[2] W. Shockley and H. Queisser, J. Appl. Phys. **32**, 510 (1961).
[3] V. M. Fridkin, Crystallogr. Rep. **46**, 654 (2001).
[4] A. M. Glass, D. von der Linde, and T. J. Negran, Appl. Phys. Lett. **25**, 233 (1974).
[5] A. G. Chynoweth, Phys. Rev. **102**, 705 (1956).
[6] F. Nastos and J. E. Sipe, Phys. Rev. B **74**, 035201 (2006).
[7] S. M. Young and A. M. Rappe, Phys. Rev. Lett. **109**, 116601 (2012).
[8] K. Nonaka, M. Akiyama, T. Hagio, and A. Takase, J. Eur. Ceram. Soc. **19**, 1143 (1999).
[9] T. Choi, S. Lee, Y. Choi, V. Kiryukhin, and S.-W. Cheong, Science **324**, 63 (2009).
[10] S. Y. Yang, J. Seidel, S. J. Byrnes, P. Shafer, C.-H. Yang, M. D. Rossel, P. Yu, Y.-H. Chu, J. F. Scott, J. W. Ager III, L. W. Martin, and R. Ramesh, Nat. Nanotech. **5**, 143 (2010).
[11] M. Alexe and D. Hesse, Nat. Commun. **2**, 256 (2011).
[12] J. Zhang, X. Su, M. Shen, Z. Dai, L. Zhang, X. He, W. Cheng, M. Cao, and G. Zou, Sci. Rep. **3**, 2109 (2013).
[13] G. Zhang, H. Wu, G. Li, Q. Huang, C. Yang, F. Huang, F. Liao, and J. Lin, Sci. Rep. **3**, 1265 (2013).
[14] J. You, Z. Hong, Y. Yang, Q. Chen, M. Cai, T.-B. Song, C.-C. Chen, S. Lu, Y. Liu, H. Zhou, and Y. Yang, ACS Nano **8**, 1674 (2014).
[15] H. J. Snaith, J. Phys. Chem. Lett. **4**, 3623 (2013).
[16] C. C. Stoumpos, C. D. Malliakas, and M. G. Kanatzidis, Inorg. Chem. **52**, 9019 (2013).
[17] W. Ji, K. Yao, and Y. C. Liang, Adv. Mater. **22**, 1763 (2010).
[18] M. Qin, K. Yao, and Y. C. Liang, Appl. Phys. Lett. **93**, 122904 (2008).
[19] D. Kan, V. Anbusathaiah, and I. Takeuchi, Adv. Mater. **23**, 1765 (2011).
[20] J. W. Bennett, I. Grinberg, and A. M. Rappe, J. Am. Chem. Soc. **130**, 17409 (2008).
[21] F. Wang, C. Di Valentin, and G. Pacchioni, J. Phys. Chem. C **116**, 8901 (2012).
[22] R. Nechache, C. Harnagea, S. Licoccia, E. Traversa, A. Ruediger, A. Pigolet, and R. Rosei, App. Phys. Lett. **98**, 202902 (2011).
[23] S. Takagi, V. R. Cooper, and D. J. Singh, Phys. Rev. B **83**, 115130 (2011).
[24] G. Y. Gou, J. W. Bennett, H. Takenaka, and A. M. Rappe, Phys. Rev. B **83**, 205115 (2011).
[25] Z. Li, Y. Shen, C. Yang, Y. Lei, Y. Guan, Y. Lin, D. Liu, and C.-W. Nan, J. Mater. Chem. A **1**, 823 (2013).
[26] Z. Zhang, P. Wu, L. Chen, and J. Wang, Appl. Phys. Lett. **96**, 012905 (2010).
[27] C.-H. Yang, D. Kan, I. Takeuchi, V. Nagarajan, and J. Seidel, Phys. Chem. Chem. Phys. **14**, 15953 (2012).

[28] R. F. Berger and J. B. Neaton, Phys. Rev. B **86**, 165211 (2012).
[29] W. S. Choi, M. F. Chisholm, D. J. Singh, T. Choi, G. E. Jellison, Jr., and H. N. Lee, Nat. Commun. **3**, 689 (2012).
[30] X. S. Xu, J. F. Ihlefeld, J. H. Lee, O. K. Ezekoye, E. Vlahos, R. Ramesh, V. Gopalan, X. Q. Pan, D. G. Schlom, and J. L. Musfeldt, Appl. Phys. Lett. **96**, 192901 (2010).
[31] I. Grinberg, D. V. West, M. Torres, G. Gou, D. M. Stein, L. Wu, G. Chen, E. M. Gallo, A. R. Akbashev, P. K. Davies, J. E. Spanier, and A. M. Rappe, Nature (London) **503**, 509 (2013).
[32] T. Qi, I. Grinberg, and A. M. Rappe, Phys. Rev. B **83**, 224108 (2011).
[33] P. Giannozzi *et al.*, J. Phys.: Condens. Matter **21**, 395502 (2009).
[34] W. Kohn and L. J. Sham, Phys. Rev. **140**, A1133 (1965).
[35] J. P. Perdew and A. Zunger, Phys. Rev. B **23**, 5048 (1981).
[36] A. M. Rappe, K. M. Rabe, E. Kaxiras, and J. D. Joannopoulos, Phys. Rev. B **41**, 1227(R) (1990).
[37] H. J. Monkhorst and J. D. Pack, Phys. Rev. B **13**, 5188 (1976).
[38] R. D. King-Smith and D. Vanderbilt, Phys. Rev. B **47**, 1651 (1993).
[39] R. Resta, Ferroelectrics **136**, 51 (1992).
[40] K. A. Johnson and N. W. Ashcroft, Phys. Rev. B **58**, 15548 (1998).
[41] J. Heyd, G. E. Scuseria, and M. Ernzerhof, J. Chem. Phys. **118**, 8207 (2003).
[42] J. Heyd, G. E. Scuseria, and M. Ernzerhof, J. Chem. Phys. **124**, 219906 (2006).
[43] M. S. Hybertsen and S. G. Louie, Phys. Rev. B **34**, 5390 (1986).
[44] J. Wróbel, K. J. Kurzydlowski, K. Hummer, G. Kresse, and J. Piechota, Phys. Rev. B **80**, 155124 (2009).
[45] Even if we assume an underestimation of 0.75 eV for the HSE06 band gap, this solid solution still exhibits E_g at the edge of the visible range, ≈0.7 eV lower than the rhombohderal phase $KNbO_3$.
[46] F. Wang, C. Di Valentin, and G. Pacchioni, ChemCatChem **4**, 476 (2012).
[47] F. Wang, I. Grinberg, and A. M. Rappe, Appl. Phys. Lett. **104**, 152903 (2014).
[48] See Supplemental Material at http://link.aps.org/supplemental/10.1103/PhysRevB.89.235105 for more information on the band structure and density of states of each strained solid solution.
[49] H. W. Eng, P. W. Barnes, B. M. Auer, and P. M. Woodward, J. Solid State Chem. **175**, 94 (2003).